Numer. Math. Theor. Meth. Appl.
doi: 10.4208/nmtma.2010.m9007

Vol. **3**, No. 4, pp. 387-404
November 2010

Gas-Kinetic BGK Scheme for Three Dimensional Magnetohydrodynamics

Huazhong Tang[1,*], Kun Xu[2] and Chunpei Cai[3]

[1] *CAPT & LMAM of School of Mathematical Sciences, Peking University, Beijing 100871, China.*
[2] *Department of Mathematics, The Hong Kong University of Science and Technology, Clear Water Bay, Kowloon, Hong Kong.*
[3] *Department of Mechanical & Aerospace Engineering, New Mexico State University, Las Cruces, NM 88003-8001, USA.*

Received 20 May 2009; Accepted (in revised version) 24 November 2009

Available online 9 September 2010

Abstract. The gas-kinetic theory based flux splitting method has been successfully proposed for solving one- and two-dimensional ideal magnetohydrodynamics by Xu et al. [*J. Comput. Phys., 1999; 2000*], respectively. This paper extends the kinetic method to solve three-dimensional ideal magnetohydrodynamics equations, where an adaptive parameter η is used to control the numerical dissipation in the flux splitting method. Several numerical examples are given to demonstrate that the proposed method can achieve high numerical accuracy and resolve strong discontinuous waves in three dimensional ideal MHD problems.

AMS subject classifications: 76M25, 76W05

Key words: The kinetic BGK scheme, magnetohydrodynamics, divergence-free condition.

1. Introduction

The ideal magnetohydrodynamics (MHD) equations are very important in modeling many flow phenomena in astrophysics, space weather, laboratory plasmas, and solar physics etc. Various high-resolution schemes have been developed for the MHD equations in the past two decades. For example, approximate Riemann solvers based on seven or eight waves eigensystems were widely used, see, e.g., [2–5, 8, 11, 16–18, 20, 23, 25, 34]. Tóth and Odstrcil in [27, 28] presented comparisons of some flux corrected transport and total variation diminishing (TVD) schemes as well as various constrained transport methods for the MHD problems. Recently, Han and Tang [13, 14] constructed a divergence-free moving mesh method for two-dimensional ideal MHD system as well as shallow-water MHD

*Corresponding author. *Email addresses:* hztang@math.pku.edu.cn (H. Tang), makxu@ust.hk (K. Xu), ccai@nmsu.edu (C. Cai)

system based on the reconstruction of the magnetic potential. Due to the non-strictly hyperbolicity of the MHD system, considerable work is required for the validation of the MHD eigensystem. Based on the particle transport mechanism, Croisille et al. and Xu et al. constructed gas-kinetic MHD solvers [10, 26, 31]. Because of the simplicity of the kinetic flux functions, the efficiency becomes one of the advantages in the kinetic approach.

The aim of this paper is to develop a higher-order kinetic BGK scheme for three-dimensional magnetohydrodynamics. The mainly difficulty in multidimensional MHD calculations is to handle the divergence-free constraint for the magnetic field $\vec{B}$, i.e. $\nabla \cdot \vec{B} = 0$. Violating this constraint leads to nonphysical plasma transport orthogonal to the magnetic field. Up to now, there are several popular approaches to enforce this condition. The first approach is the projection method of Brackbill and Barnes [7]. In order to impose the divergence free condition for the magnetic field $\vec{B}$, a correction method is enforced in solving the Poisson equation for the scalar potential ϕ, such as $\nabla^2\phi + \nabla \cdot \mathbf{B} = 0$, to obtain the corrected magnetic field $\mathbf{B}^c$ through $\mathbf{B}^c = \mathbf{B} + \nabla\phi$, where $\mathbf{B}^c$ becomes a divergence-free field and will be used in the next time step. This technique is commonly used in many MHD solvers [7, 15, 26, 33]. However, in general, the Poisson solver is time consuming on an unstructured mesh or in curvilinear coordinates; and conservation of the total energy may slightly be lost.

The second approach is the eight-wave formulation of the MHD equations suggested by Powell and Aslan [1, 19], who added source terms, which are proportional to the magnetic divergence, to the right hand side of the momentum and total energy equations in the ideal MHD system, respectively. The main disadvantage of this approach is that the 8-wave formulation of the MHD equations becomes non-conservative so that incorrect results may be produced in problems containing strong shocks [27].

The third approach is the constrained transport (CT) method of Evans and Hawley [12], in which a particular finite difference method was constructed on a staggered mesh, maintaining a specific discretization of $\nabla \cdot \vec{B}$. Because of its simplicity, this approach becomes rather popular in recent years, see, e.g., [6, 11, 22]. Tóth [27] introduced a finite-volume interpretation of the CT schemes that place all of the variables at the cell center. However, the idea seems to be difficult to apply to an adaptive mesh (refinement mesh or moving mesh). It is worth noting that most of the existing CT methods are designed on a rectangle or cubic mesh. Another way to keep the magnetic field divergence-free is to directly solve the magnetic potential equations instead of the induction equation in the ideal MHD system, see [9, 12, 21]. The disadvantage of this approach is that the order of spatial derivatives increases by one, which reduces the order of accuracy by one.

The paper is organized as follows. Section 2 introduces the governing equations for the three-dimensional ideal MHDs. Section 3 develops a higher-order kinetic BGK scheme for three-dimensional magnetohydrodynamics. The adjust parameter η is adaptively defined in the BGK scheme. We correct the magnetic field of the base MHD solver by the projection method. Numerical experiments are carried out in Sections 4 on two benchmark examples, which are the spherical explosion problem and the spherical cloud and shock wave interaction problem. Finally, we conclude this work by giving a few remarks in Section 5.

2. Governing equations

Let us use (x_1, x_2, x_3) to denote the Cartesian coordinate vector. The three-dimensional ideal magnetohydrodynamical (MHD) equations are

$$\begin{aligned}
&\rho_t + \nabla\cdot(\rho\vec{u}) = 0,\\
&(\rho\vec{u})_t + \nabla\cdot(\rho\vec{u}\otimes\vec{u} + p_{\text{tot}}\mathbf{I} - \vec{B}\otimes\vec{B}) = 0,\\
&E_t + \nabla\cdot\left(\vec{u}(E + p_{\text{tot}}) - (\vec{u}\cdot\vec{B})\vec{B}\right) = 0,\\
&\vec{B}_t + \nabla\cdot(\vec{u}\otimes\vec{B} - \vec{B}\otimes\vec{u}) = 0,
\end{aligned} \tag{2.1}$$

where $\nabla = (\partial_{x_1}, \partial_{x_2}, \partial_{x_3})^T$, ρ, $\vec{u} = (u_1, u_2, u_3)^T$, $\vec{B} = (B_1, B_2, B_3)^T$ denote mass density, fluid velocity vector, and magnetic field, respectively. The total pressure is equal to a sum of the gas pressure and the magnetic pressure, i.e. $p_{\text{tot}} = p_{\text{gas}} + p_{\text{mag}}$ with $p_{\text{mag}} = \frac{1}{2}|\vec{B}|^2$, $\mathbf{I}$ denotes a rank-2 unit tensor. The total energy density includes thermal, kinetic, and magnetic energies,

$$E = \rho e + \frac{1}{2}(\rho u^2 + B^2), \tag{2.2}$$

where ρe is the thermal energy density, $u^2 = \sum_{i=1}^3 u_i^2$, $B^2 = \sum_{i=1}^3 B_i^2$. For an ideal gas, the thermal energy is related to the gas pressure through the relation

$$p = (\gamma - 1)\rho e. \tag{2.3}$$

The MHD equations (2.1) represent conservation of mass, momentum, total energy, and magnetic field, respectively, and are combined with (2.2) and (2.3) to form a closed system. Solutions of the MHD equations must also satisfy a divergence-free constraint on the magnetic field,

$$\nabla\cdot\vec{B} = 0, \tag{2.4}$$

due to the absence of monopoles. if the initial magnetic field is divergence-free. It is imposed by Maxwell's equations.

It is well known that (2.1) allows four kinds of waves: the entropy wave associated with wave speed u_n, and the slow, Alfven, and fast waves. For example, the wave speeds for the slow, Alfven, and fast waves in x_1-direction are respectively

$$u_1 \pm c_s, \quad u_1 \pm c_a, \quad \text{and} \quad u_1 \pm c_f,$$

where c_s, c_a and c_f are defined by

$$\begin{aligned}
c_f &:= \frac{1}{\sqrt{2}}\left((c_p^2 + c_a^2 + c_2^2 + c_3^2) + \sqrt{(c_p^2 + c_a^2 + c_2^2 + c_3^2) - 4c_p^2c_a^2}\right)^{1/2},\\
c_s &:= \frac{1}{\sqrt{2}}\left((c_p^2 + c_a^2 + c_2^2 + c_3^2) - \sqrt{(c_p^2 + c_a^2 + c_2^2 + c_3^2) - 4c_p^2c_a^2}\right)^{1/2},
\end{aligned}$$

and

$$c_p^2 = \gamma\frac{p}{\rho}, \quad c_a^2 = \frac{B_1^2}{\rho}, \quad c_2^2 = \frac{B_2^2}{\rho}, \quad c_3^2 = \frac{B_3^2}{\rho}.$$

3. Numerical methods

In this section we extend the gas-kinetic flux splitting method in [26,31] to the three-dimensional ideal MHDs. For the sake of simplicity, we restrict our attention to the structured hexahedral mesh, see Fig. 1, denoted by $\{A_{i+\frac{1}{2},j+\frac{1}{2},k+\frac{1}{2}}\}$, which is covering the physical domain Ω. We also use S^m, $m=1,2,\cdots,6$, to denote six surfaces of the control volume $A_{i+\frac{1}{2},j+\frac{1}{2},k+\frac{1}{2}}$, and $\vec{n}^m$ to denote corresponding unit outward normal vector on S^m, for example,

$$S^1 := \vec{x}_{i,j,k}\vec{x}_{i,j+1,k}\vec{x}_{i,j+1,k+1}\vec{x}_{i,j,k+1}, \qquad S^2 := \vec{x}_{i+1,j,k}\vec{x}_{i+1,j+1,k}\vec{x}_{i+1,j+1,k+1}\vec{x}_{i+1,j,k+1}.$$

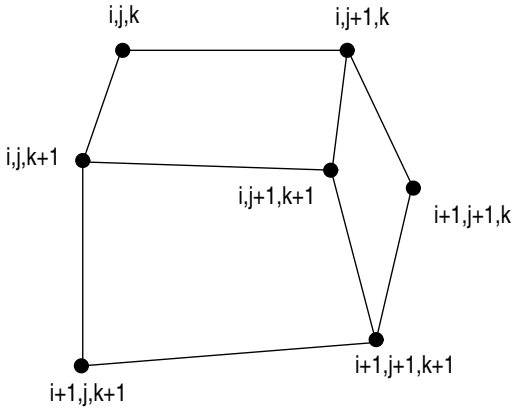

Figure 1: The hexahedral control volume in three-dimensional space.

3.1. Spatial discretization

For convenience, we rewrite the MHD equations (2.1) in the following compact form:

$$\frac{\partial \vec{U}}{\partial t} + \sum_{l=1}^{3} \frac{\partial \vec{F}_l}{\partial x_l} = 0, \tag{3.1}$$

where

$$\vec{U} = \begin{pmatrix} \rho \\ \rho u_1 \\ \rho u_2 \\ \rho u_3 \\ E \\ B_1 \\ B_2 \\ B_3 \end{pmatrix}, \qquad \vec{F}_1(\vec{U}) = \begin{pmatrix} \rho u_1 \\ \rho u_1^2 + p_{\text{tot}} - B_1^2 \\ \rho u_1 u_2 - B_1 B_2 \\ \rho u_1 u_3 - B_1 B_3 \\ u_1(E + p_{\text{tot}}) - B_1(\vec{u}\cdot\vec{B}) \\ 0 \\ u_1 B_2 - u_2 B_1 \\ u_1 B_3 - u_3 B_1 \end{pmatrix},$$

$$\vec{F}_2(\vec{U}) = \begin{pmatrix} \rho u_2 \\ \rho u_1 u_2 - B_1 B_2 \\ \rho u_2^2 + p_{\text{tot}} - B_2^2 \\ \rho u_2 u_3 - B_2 B_3 \\ u_2(E + p_{\text{tot}}) - B_2(\vec{u}\cdot\vec{B}) \\ u_2 B_1 - u_1 B_2 \\ 0 \\ u_2 B_3 - u_3 B_2 \end{pmatrix}, \quad \vec{F}_3(\vec{U}) = \begin{pmatrix} \rho u_3 \\ \rho u_1 u_3 - B_1 B_3 \\ \rho u_2 u_3 - B_2 B_3 \\ \rho u_3^2 + p_{\text{tot}} - B_3^2 \\ u_3(E + p_{\text{tot}}) - B_3(\vec{u}\cdot\vec{B}) \\ u_3 B_1 - u_1 B_3 \\ u_3 B_2 - u_2 B_3 \\ 0 \end{pmatrix}. \tag{3.2}$$

Integrating (3.1) over the control volume $A_{i+\frac{1}{2},j+\frac{1}{2},k+\frac{1}{2}}$ and using the divergence theorem and the mid-point integral formula gives

$$\frac{\partial}{\partial t}\iint_{A_{i+\frac{1}{2},j+\frac{1}{2},k+\frac{1}{2}}} \vec{U}\,\mathrm{d}V + \sum_{m=1}^{6} \vec{F}\left(\vec{n}^m; \vec{U}(S^m)\right)\cdot|S^m| = 0 \tag{3.3}$$

where $\vec{F}\left(\vec{n}^m; \vec{U}\right) = \vec{F}_1 n_1^m + \vec{F}_2 n_2^m + \vec{F}_3 n_3^m$ denotes the flux function across the cell interface in the normal $\vec{n}^m = (n_1^m, n_2^m, n_3^m)$ direction, which can be explicitly expressed as

$$\vec{F}\left(\vec{n}; \vec{U}\right) = \begin{pmatrix} \rho u_n \\ \rho u_n u_1 + p_{\text{tot}} n_1 - B_1 B_n \\ \rho u_n u_2 + p_{\text{tot}} n_2 - B_2 B_n \\ \rho u_n u_3 + p_{\text{tot}} n_3 - B_3 B_n \\ u_n(E + p_{\text{tot}}) - (\vec{u}\cdot\vec{B})B_n \\ u_n B_1 - u_1 B_n \\ u_n B_2 - u_2 B_n \\ u_n B_3 - u_3 B_n \end{pmatrix}, \tag{3.4}$$

where $u_n = \vec{u}\cdot\vec{n}$ and $B_n = \vec{B}\cdot\vec{n}$, $\vec{U}(S)$ denotes value of the solution at the centroid of the surface S. Note that the superscript m has been omitted here.

Using a suitable numerical flux to replace the flux $\vec{F}\left(\vec{n}^m; \vec{U}\right)$ in (3.3), we get the following semi-discrete finite volume scheme

$$\frac{\mathrm{d}}{\mathrm{d}t}\overline{\vec{U}}_{i+\frac{1}{2},j+\frac{1}{2},k+\frac{1}{2}}(t) = -\frac{1}{|A_{i+\frac{1}{2},j+\frac{1}{2},k+\frac{1}{2}}|}\sum_{m=1}^{6} \widehat{\vec{F}}\left(\vec{n}^m; \vec{U}^L(S^m), \vec{U}^R(S^m)\right)\cdot|S^m|, \tag{3.5}$$

where $\vec{U}^L(S^m)$ and $\vec{U}^R(S^m)$ are the left and right states across the interface S^m, and defined by

$$\vec{U}^L(S^m) = \overline{\vec{U}}_{i+\frac{1}{2},j+\frac{1}{2},k+\frac{1}{2}} + \frac{1}{2}\vec{S}_{i+\frac{1}{2},j+\frac{1}{2},k+\frac{1}{2}}, \tag{3.6}$$

$$\vec{U}^R(S^m) = \overline{\vec{U}}_{i+\frac{3}{2},j+\frac{1}{2},k+\frac{1}{2}} - \frac{1}{2}\vec{S}_{i+\frac{3}{2},j+\frac{1}{2},k+\frac{1}{2}}, \tag{3.7}$$

and $\vec{S}_{i+\frac{1}{2},j+\frac{1}{2},k+\frac{1}{2}}$ is the limited slope in the i-direction, which has the form

$$\vec{S}_{i+\frac{1}{2},j+\frac{1}{2},k+\frac{1}{2}} = \mathrm{vLL}\Big(\overline{\vec{U}}_{i+\frac{3}{2},j+\frac{1}{2},k+\frac{1}{2}} - \overline{\vec{U}}_{i+\frac{1}{2},j+\frac{1}{2},k+\frac{1}{2}}, \overline{\vec{U}}_{i+\frac{1}{2},j+\frac{1}{2},k+\frac{1}{2}} - \overline{\vec{U}}_{i-\frac{1}{2},j+\frac{1}{2},k+\frac{1}{2}}\Big).$$

Here the function $\mathrm{vLL}(a,b)$ denotes the van Leer limiter [30], defined by

$$\mathrm{vLL}(a,b) = \big(\mathrm{sign}(a) + \mathrm{sign}(b)\big)\frac{|ab|}{|a|+|b|+\varepsilon},$$

where the small positive parameter ε is used to avoid zero in the denominator. In this paper, we take ε as 10^{-10}.

3.2. Time discretization and magnetic correction

The time derivatives in (3.5) are discretized using a second-order accurate Heun method, see, e.g., [24]:

$$\begin{aligned}
\vec{U}^{(1)} &= \vec{U}^n + \Delta t_n \vec{L}(\vec{U}^n),\\
\vec{U}^{(2)} &= \vec{U}^{(1)} + \Delta t_n \vec{L}(\vec{U}^{(1)}),\\
\vec{U}^{*} &= \frac{1}{2}(\vec{U}^{(2)} + \vec{U}^n),
\end{aligned} \tag{3.8}$$

where $\vec{L}(\vec{U})$ denotes the term on the right hand side of (3.5), and all subscripts have been omitted.

At each time level, the computed magnetic fields are corrected by the projection method [7] as follows

$$(\rho, \rho\vec{u})^{n+1} = (\rho, \rho\vec{u})^{*}, \tag{3.9}$$

$$\vec{B}^{n+1} = \vec{B}^{*} + \nabla_h \phi, \tag{3.10}$$

$$E^{n+1} = E^{*} + \frac{1}{2}(|\vec{B}^{n+1}|^2 - |\vec{B}^{*}|^2), \tag{3.11}$$

where ∇_h denotes the approximate gradient operator.

Other magnetic corrections are also considered, but their implementation should be very careful because of some possible limitations. For example, the central difference method of Tóth on the structured hexahedral mesh becomes

$$(B_1)^{n+1} = (B_1)^n - \Delta t_n(-\mathscr{D}_2\Omega_3 + \mathscr{D}_3\Omega_2)^{n+1/2}, \tag{3.12}$$

$$(B_2)^{n+1} = (B_2)^n - \Delta t_n(\mathscr{D}_1\Omega_3 - \mathscr{D}_3\Omega_1)^{n+1/2}, \tag{3.13}$$

$$(B_3)^{n+1} = (B_3)^n - \Delta t_n(-\mathscr{D}_1\Omega_2 + \mathscr{D}_2\Omega_1)^{n+1/2}, \tag{3.14}$$

where $(\Omega_1,\Omega_2,\Omega_3)^T = \vec{\Omega} = \vec{u}\times\vec{B}$, $\mathscr{D}_m$ denotes a central difference approximation of the partial differential operator ∂_{x_m}, $m = 1,2,3$, and

$$\vec{\Omega}^{n+1/2} = \frac{1}{2}\Big((\vec{u}\times\vec{B})^n + (\vec{u}\times\vec{B})^{*}\Big).$$

3.3. Gas-kinetic theory based flux splitting

In the following, we present the gas-kinetic theory based flux splitting method. Following the idea in [31] and [26], we only need evaluate the local one-dimensional macroscopic flux function through each cell interface based on the gas-kinetic theory, in which the flux is associated with the particle transport across a cell interface. For the one-dimensional flow, such as in the $\vec{n}$-direction, the normal component of the particle velocity v_n is important in the determination of the flux function across the cell interface with a normal direction $\vec{n}$. Other quantities can be considered as passive scalars, which are transported with the $\vec{n}$-direction particle motion. Since particles are randomly distributed around an average velocity, these moving particles in the $\vec{n}$-direction can be favorably described by a Maxwell-Boltzmann distribution function

$$g = \rho \left(\frac{\lambda}{\pi}\right)^{1/2} e^{-\lambda(v_n-u_n)^2},$$

where λ is the normalization factor of the distribution of random velocity, which is related to the local temperature of the gas flow. For the MHD, both the gas and the magnetic field contribute to the total pressure p_{tot} and the total internal energy is a combination of gas and magnetic energy. Since the pressure is related to the integration of the particle distribution function g

$$\int_{-\infty}^{+\infty} (v_n-u_n)^2 g \, \mathrm{d}v_n = \frac{\rho}{2\lambda},$$

the value of λ is uniquely determined by $\lambda = \rho/2p_{\text{tot}}$.

After determining λ, we can split the particles into two groups in the $\vec{n}$-direction according to $v_n > 0$ and $v_n < 0$. As a result, the three-dimensional MHD flux function in the $\vec{n}$-direction becomes

$$\vec{F}(\vec{n};\vec{U}) = \vec{F}^{+}(\vec{n};\vec{U}) + \vec{F}^{-}(\vec{n};\vec{U}),$$

where the positive and negative parts are

$$\vec{F}^{\pm}(\vec{n};\vec{U}) = \begin{pmatrix} \rho \\ \rho u_1 \\ \rho u_2 \\ \rho u_3 \\ E + p_{\text{tot}} - B_n^2 \\ B_1 - n_1 B_n \\ B_2 - n_2 B_n \\ B_3 - n_3 B_n \end{pmatrix} < v_n^1 >_{\pm} + \begin{pmatrix} 0 \\ p_{\text{tot}} n_1 - B_1 B_n \\ p_{\text{tot}} n_2 - B_2 B_n \\ p_{\text{tot}} n_3 - B_3 B_n \\ u_n B_n^2 - (\vec{u}\cdot\vec{B}) B_n \\ (n_1 u_n - u_1) B_n \\ (n_2 u_n - u_2) B_n \\ (n_3 u_n - u_3) B_n \end{pmatrix} < v_n^0 >_{\pm}. \tag{3.15}$$

Here the moments $< v_n^0 >_{\pm}$ and $< v_n^1 >_{\pm}$ are defined by

$$< v_n^0 >_{\pm} = \frac{1}{2}\mathrm{erfc}(\mp\sqrt{\lambda}u_n),$$

$$< v_n^1 >_{\pm} = u_n < v_n^0 >_{\pm} \pm \frac{1}{2\sqrt{\lambda\pi}} e^{-\lambda u_n^2}.$$

As a result, the splitting flux function for the MHD equations across the cell interface S^1 becomes

$$\widehat{\vec{F}}(\vec{n}^1;\vec{U}) = \vec{F}^+\left(\vec{n}^1;\vec{U}_{i-\frac{1}{2},j+\frac{1}{2},k+\frac{1}{2}}\right) + \vec{F}^-\left(\vec{n}^1;\vec{U}_{i+\frac{1}{2},j+\frac{1}{2},k+\frac{1}{2}}\right). \tag{3.16}$$

The above MHD flux splitting formulation goes back to the kinetic flux-vector splitting (KFVS) method developed by Croisille et al. in the one-dimensional case [10]. This KFVS-type MHD method is very robust, but over-diffusive, especially in the case with coarse mesh. To reduce the numerical dissipation, Xu [31] implemented a particle collision mechanism in the above flux transporting process. The idea is to obtain an "equilibrium state" $\vec{U}^e$ at the cell interface by combining the left and right moving beams and use this state to get an equilibrium flux function $\vec{F}^e(\vec{n};\vec{U}^e)$ through the flux definition in (3.4). The equilibrium state $\vec{U}^e_{i,j+\frac{1}{2},k+\frac{1}{2}}$ at the cell interface, such as S^1, can be constructed as

$$\vec{U}^e_{i,j+\frac{1}{2},k+\frac{1}{2}} = \vec{U}^+_{i-\frac{1}{2},j+\frac{1}{2},k+\frac{1}{2}} + \vec{U}^-_{i+\frac{1}{2},j+\frac{1}{2},k+\frac{1}{2}}, \tag{3.17}$$

where $\vec{n}^1 := (n_1, n_2, n_3)$, and

$$\vec{U}^{\pm} = \begin{pmatrix} 0 \\ \rho n_1 \\ \rho n_2 \\ \rho n_3 \\ \frac{1}{2}\rho u_n^2 \\ 0 \\ 0 \\ 0 \end{pmatrix} < \nu_n^1 >_{\pm} + \begin{pmatrix} \rho \\ \rho(u_1 - n_1 u_n) \\ \rho(u_2 - n_2 u_n) \\ \rho(u_3 - n_3 u_n) \\ E - \frac{1}{2}\rho u_n^2 \\ B_x \\ B_y \\ B_z \end{pmatrix} < \nu_n^0 >_{\pm}. \tag{3.18}$$

Then, the final numerical flux across the cell interface S^1 is given by

$$\widehat{\vec{F}}_{i,j+\frac{1}{2},k+\frac{1}{2}} = (1-\eta)\widehat{\vec{F}}^e_{i,j+\frac{1}{2},k+\frac{1}{2}} + \eta\widehat{\vec{F}}^f_{i,j+\frac{1}{2},k+\frac{1}{2}}, \tag{3.19}$$

where

$$\widehat{\vec{F}}^f_{i,j+\frac{1}{2},k+\frac{1}{2}} = \vec{F}^+\left(\vec{n}^1;\vec{U}_{i-\frac{1}{2},j+\frac{1}{2},k+\frac{1}{2}}\right) + \vec{F}^-\left(\vec{n}^1;\vec{U}_{i+\frac{1}{2},j+\frac{1}{2},k+\frac{1}{2}}\right)$$

denotes the splitting flux function defined in (3.15),

$$\widehat{\vec{F}}^e_{i,j+\frac{1}{2},k+\frac{1}{2}} = \vec{F}\left(\vec{n}^1;\vec{U}^e_{i,j+\frac{1}{2},k+\frac{1}{2}}\right)$$

is the equilibrium flux function, see (3.4), and η is an adaptive parameter, $0 \le \eta \le 1$. Physically, η should be an adaptive parameter related to the real flow situation. For example, in the strong discontinuity region, it must have a large value to account for the non-equilibrium property. Based on this guide line, we design the adaptive parameter η as follows

$$\eta_{i,j+\frac{1}{2},k+\frac{1}{2}} = \max\left\{\eta_0, 1 - e^{-\alpha|(p_{\mathrm{mag}})_{i+\frac{1}{2},j+\frac{1}{2},k+\frac{1}{2}} - (p_{\mathrm{mag}})_{i-\frac{1}{2},j+\frac{1}{2},k+\frac{1}{2}}|}\right\}, \tag{3.20}$$

which ensures that $\eta_{i,j+\frac{1}{2},k+\frac{1}{2}} = 1$ when the magnetic pressure is strongly discontinuous, otherwise $\eta_{i,j+\frac{1}{2},k+\frac{1}{2}} = \eta_0$.

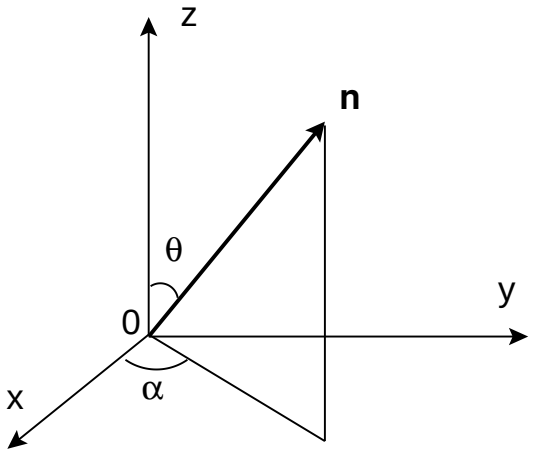

Figure 2: The unit vector $\vec{n}$ in three-dimensional space.

Remark 3.1. In construction of the equilibrium state (3.17) we need the local 3D rotational transformation according to the unit normal vector $\vec{n}$ of the cell interface, see Fig. 2.

Because the 3D unit vector $\vec{n} = (n_1, n_2, n_3)$ may be denoted as

$$n_1 = \sin\theta\cos\alpha, \quad n_2 = \sin\theta\sin\alpha, \quad n_3 = \cos\theta, \tag{3.21}$$

where θ and α are the angles between the vector $\vec{n}$ and x_3-axis and x_1-axes, respectively, we have a 3D rotational transformation as follows

$$\begin{pmatrix} u_n \\ u_\tau \\ u_b \end{pmatrix} = \begin{pmatrix} \sin\theta\cos\alpha & \sin\theta\sin\alpha & \cos\theta \\ -\sin\alpha & \cos\alpha & 0 \\ -\cos\theta\cos\alpha & -\cos\theta\sin\alpha & \sin\theta \end{pmatrix} \begin{pmatrix} u_1 \\ u_2 \\ u_3 \end{pmatrix}. \tag{3.22}$$

Its inversion becomes

$$\begin{pmatrix} u_1 \\ u_2 \\ u_3 \end{pmatrix} = \begin{pmatrix} \sin\theta\cos\alpha & -\sin\alpha & -\cos\theta\cos\alpha \\ \sin\theta\sin\alpha & \cos\alpha & -\cos\theta\sin\alpha \\ \cos\theta & 0 & \sin\theta \end{pmatrix} \begin{pmatrix} u_n \\ u_\tau \\ u_b \end{pmatrix}. \tag{3.23}$$

4. Numerical experiments

In this section we apply the present BGK scheme to two 3D ideal MHD problems in order to demonstrate its performance. The problems are the spherical explosion and the shock wave and the spherical cloud interaction. Throughout our computations, we always take $\gamma = 5/3$, the CFL number $cfl = 0.124$, $\alpha = 10$, and use 100^3 uniform cells to partition the physical domain $\Omega = [0,1]^3$. We take $\eta_0 = 0.7$ generally, unless otherwise stated.

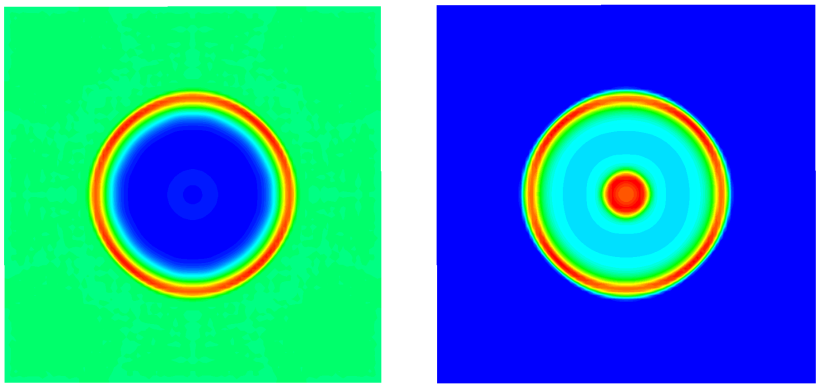

(a) Density (b) Gas pressure

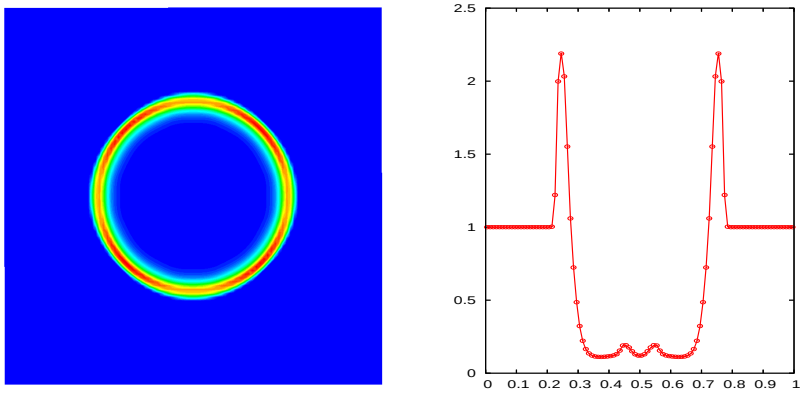

(c) Kinetic energy (d) Density along $y = z = 0.5$

Figure 3: Example 4.1: the solutions at $t = 0.03$ for $B_2^0 = 0$. The CFL number is 0.124, and 100^3 cells are used.

Example 4.1. The first example is to solve the spherical explosion problem within the domain $[0,1]^3$, which is an extension of two-dimensional problem in [26]. The initial data are set as

$$\vec{W} = \begin{cases} (1,0,0,0,100,0,B_2^0,0), & \text{if } |\vec{x} - \vec{x}_0| < 0.1, \\ (1,0,0,0,1,0,B_2^0,0), & \text{otherwise}, \end{cases} \tag{4.1}$$

where $\vec{W} = (\rho, u_1, u_2, u_3, p, B_1, B_2, B_3)$. Here $\vec{x}_0$ denotes the center of the cube. In this example, we test three cases with $B_2^0 = 0, 5/\sqrt{\pi}$ and $50/\sqrt{\pi}$, respectively.

Fig. 3 shows the solutions at $t = 0.03$ for $B_2^0 = 0$. We also give a comparison of the KFVS and BGK schemes in Fig. 3(d). We see that they are almost fully identical. It is worth noting that the strength of the shock in the spherical explosion is weaker than that in the cylindrical explosion. In this case, $\eta_{i,j+\frac{1}{2},k+\frac{1}{2}} \equiv \eta_0$ automatically.

Fig. 4 show the contours of the density, pressure, the magnetic pressure, and the kinetic energy at $t = 0.03$ in the plane $z = 0.5$ for $B_2^0 = 5/\sqrt{\pi}$. A comparison of the KFVS and BGK schemes is given in Fig. 5.

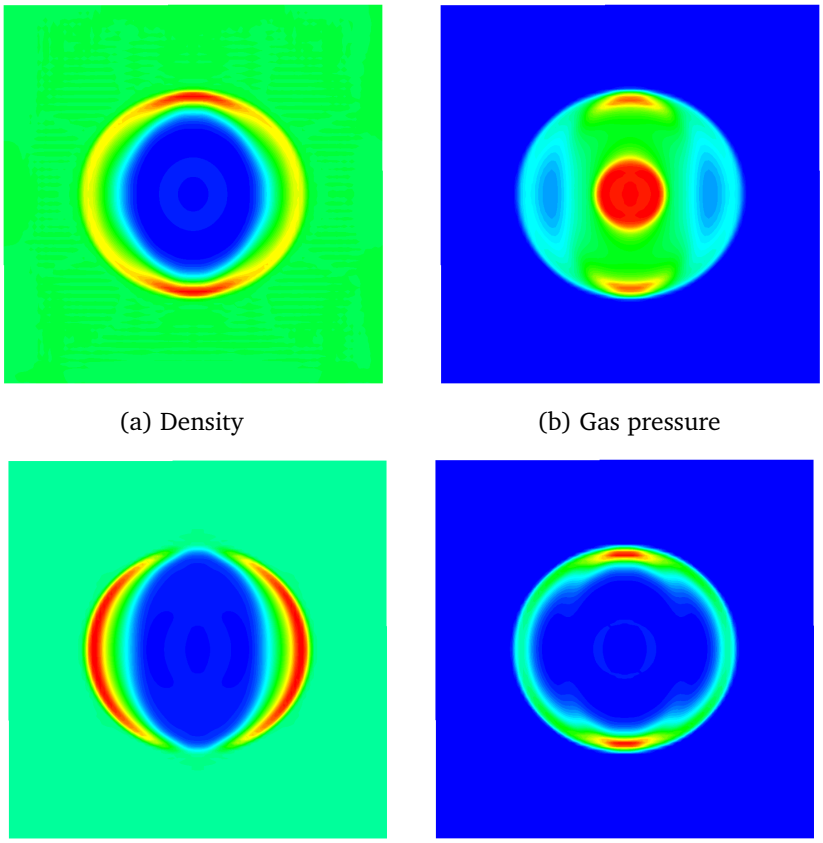

(a) Density (b) Gas pressure

(c) Magnetic pressure (d) Kinetic energy

Figure 4: Same as Fig. 3, except for $B_2^0 = 5/\sqrt{\pi}$.

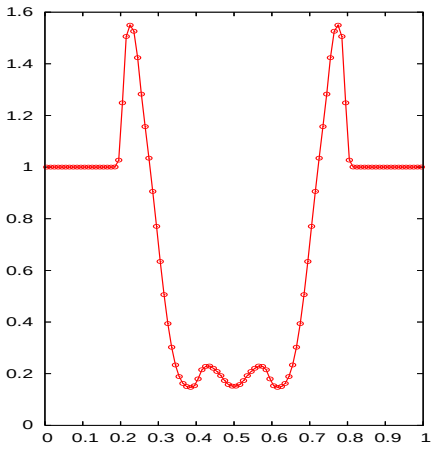

Figure 5: Example 4.1: The densities at $t = 0.03$ for $B_2^0 = 5/\sqrt{\pi}$ along the line $y = 0.5$ in the plane $z = 0.5$ obtained using KFVS scheme ($\eta = 1$, solid line) and the BGK scheme (adaptive choice of η, symbol "o").

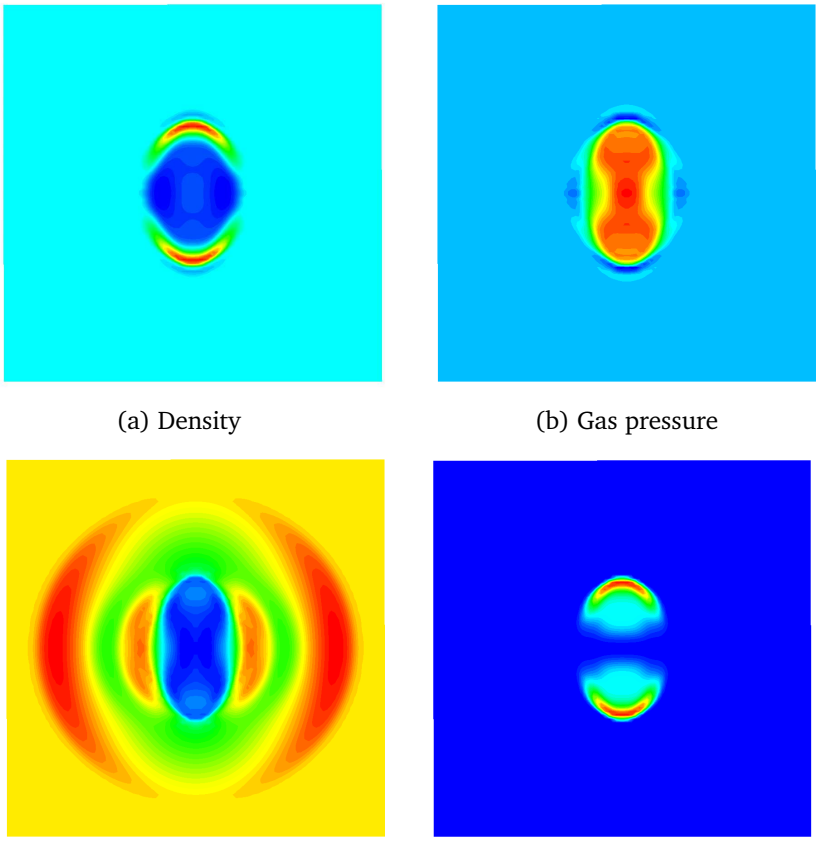

(a) Density (b) Gas pressure

(c) Magnetic pressure (d) Kinetic energy

Figure 6: Same as Fig. 3, except for $B_2^0 = 50/\sqrt{\pi}$ and $t = 0.0105$.

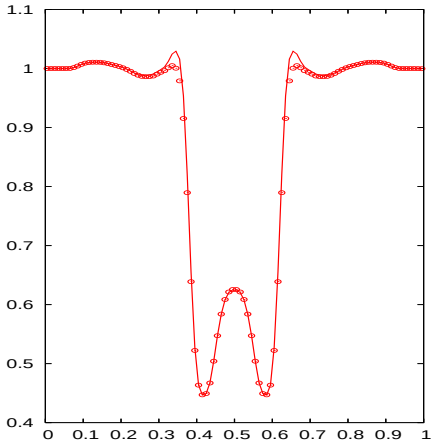

Figure 7: Example 4.1: The densities at $t = 0.0105$ for $B_2^0 = 5/\sqrt{\pi}$ along the line $y = 0.5$ in the plane $z = 0.5$ obtained using KFVS scheme ($\eta = 1$, solid line) and the BGK scheme (adaptive choice of η, symbol "$\circ$"). We have used 100^3 cells.

Fig. 6 show the contours of the density, pressure, the magnetic pressure, and the kinetic energy at $t = 0.0105$ in the plane $z = 0.5$ for $B_2^0 = 50/\sqrt{\pi}$. From Fig. 7, we see certain differences between the KFVS and BGK results. In this case, we have taken $\eta_0 = 0.9$. Actually, the control of numerical dissipation through the parameter η will be mostly effective for the smooth viscous and heat conduction flow simulation. The small difference for the strong shock cases, such as the current example, is reasonable because a large amount of dissipation is introduced already in the strong discontinuous regions.

Example 4.2. The second example is to solve the shock wave and spherical cloud interaction problem. A similar problem in two dimensions has been considered in several papers [11, 14]. Initially a right-moving plane shock is set at $x = 0.05$ with the left and right constant states:

$$\vec{W} = \begin{cases} (3.86859, 11.2536, 0, 0, 167.345, 0, 2.1826182, -2.1826182), & \text{if } x_1 < 0.05, \\ (1, 0, 0, 0, 1, 0, 0.56418985, 0.56418985), & \text{otherwise.} \end{cases} \tag{4.2}$$

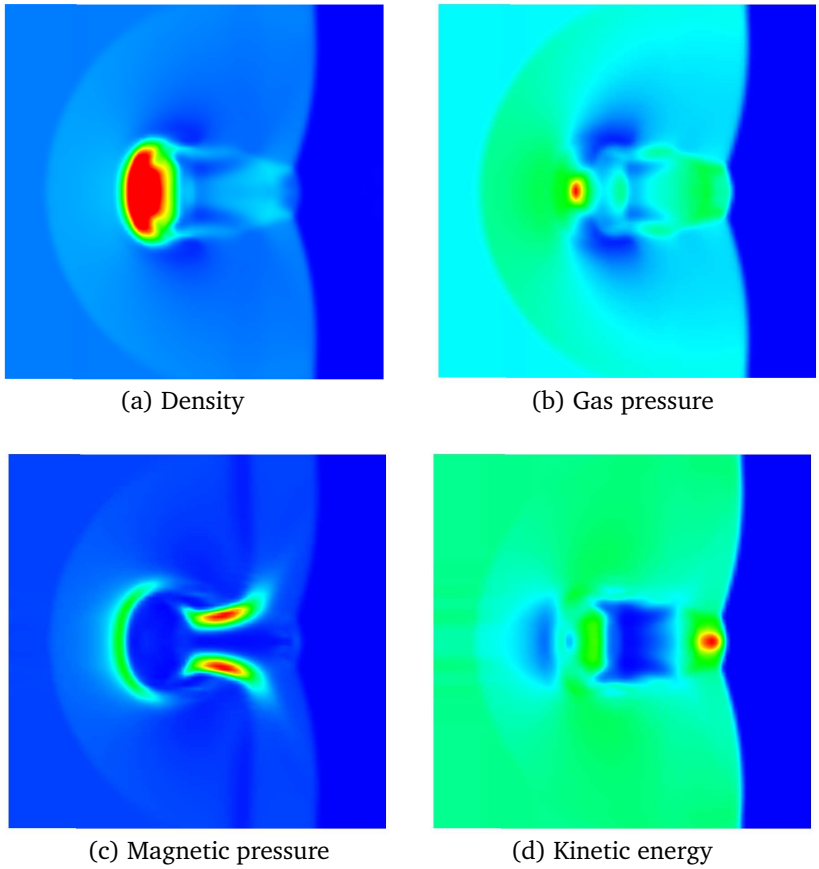

(a) Density (b) Gas pressure

(c) Magnetic pressure (d) Kinetic energy

Figure 8: Example 4.2: the contour surfaces of the density, pressure, the magnetic pressure, and the kinetic energy at $t = 0.05$ in the plane $z = 0.5$.

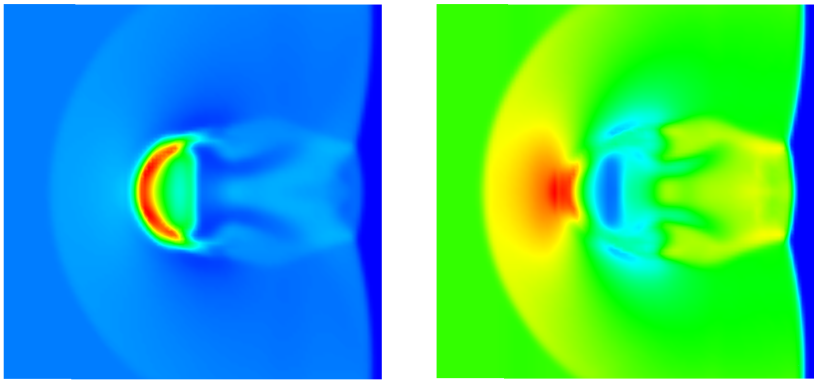

(a) Density (b) Gas pressure

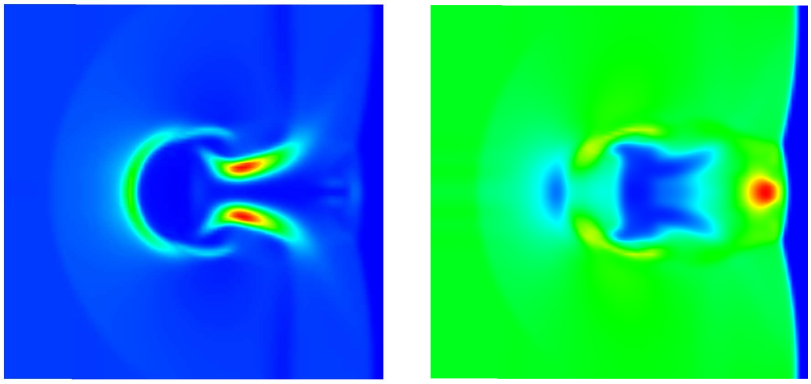

(c) Magnetic pressure (d) Kinetic energy

Figure 9: Same as Fig. 8 except for $t = 0.06$.

At the same time, a 10 times denser spherical cloud is in the downstream section of the shock wave and initially centered at (0.25,0.5,0.5) with a radius of 0.15 and a density of 10. We assume that the dense cloud is in hydrostatic equilibrium with the surrounding fluid. Figs. 8 and 9 show the contour surfaces of the density, pressure, the magnetic pressure, and the kinetic energy at $t = 0.05$ and 0.06 in the plane $z = 0.5$. Fig. 11 gives the densities along the straight line $y = z = 0.5$, where the symbol "circle" and solid line denote the solutions obtained by using the BGK scheme and the KFVS scheme, respectively. In comparison with the results of Fig. 8 in [29], the current kinetic scheme has less dissipation than that in the central finite volume method.

In Fig. 10, we present the corresponding two-dimensional solutions of the shock and cylindrical bubble interaction problem, which are obtained by using 2D BGK scheme developed in [26]. Comparing them with those shown in Fig. 8, we see that the wave patterns are almost same, but the reflecting shock becomes stronger than that in 3D case. Also, obvious differences in the bubble collapse and the distance between the reflective shock and the bubble can be observed.

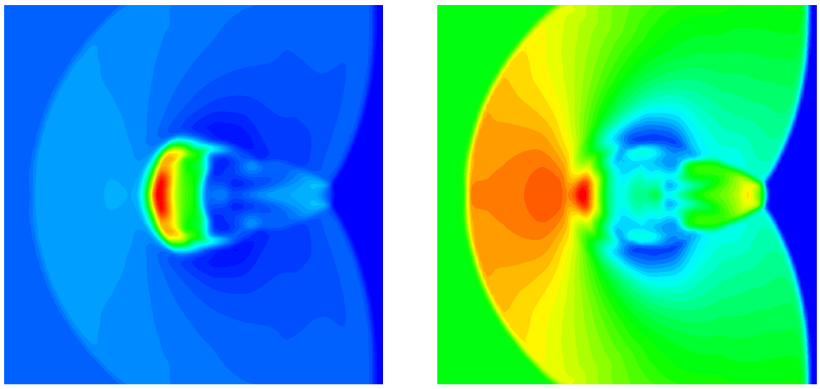

(a) Density (b) Gas pressure

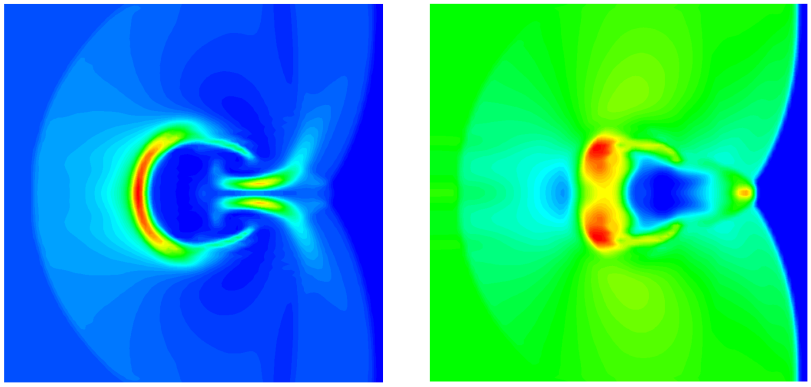

(c) Magnetic pressure (d) Kinetic energy

Figure 10: The contour surfaces of the solutions at $t = 0.06$ for the interaction between the shock and cylindrical bubble. The results are obtained by using 2D BGK scheme [26] with 100^2 cells.

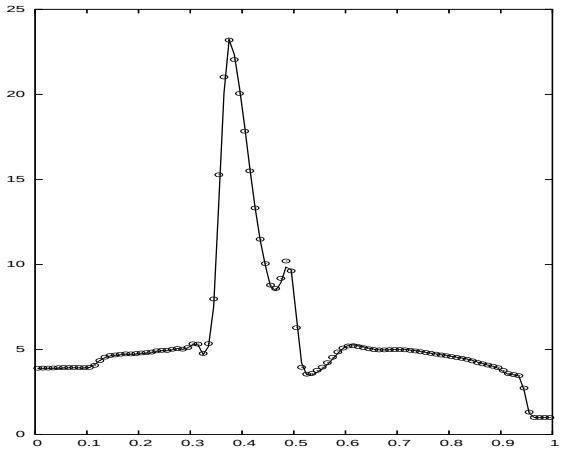

Figure 11: Example 4.2: the densities along the straight line $y = z = 0.5$. The symbol "circle" and solid line denote the solutions obtained using $\eta = 0.7$ and 1, respectively.

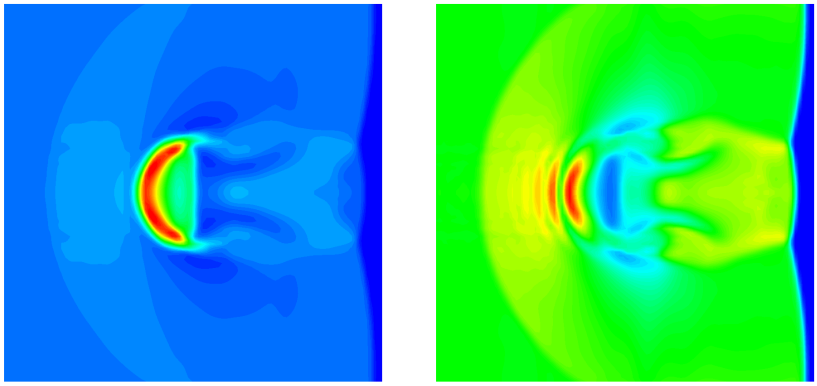

(a) Density (b) Gas pressure

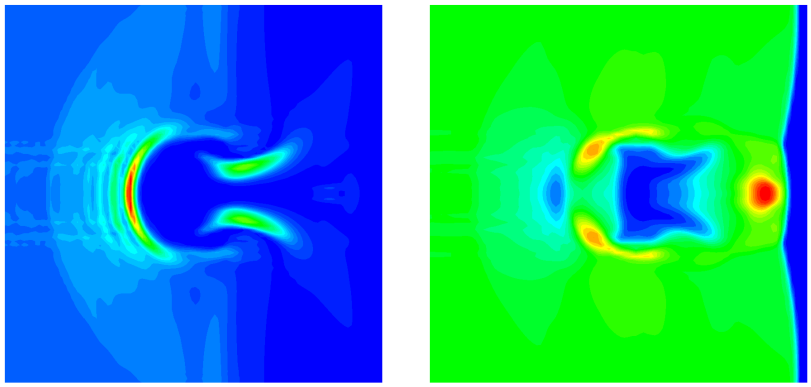

(c) Magnetic pressure (d) Kinetic energy

Figure 12: Same as Fig. 9 except using the central difference magnetic correction method of Tóth [28] to update magnetic field.

5. Discussion and conclusions

This paper presents a higher-order kinetic BGK scheme for three-dimensional ideal magnetohydrodynamics (MHD). The current scheme is a multi-dimensional extension of the gas-kinetic theory based flux splitting method proposed by Xu et al. in [26,31], for solving one- and two-dimensional ideal MHDs. Moreover, the parameter η in the gas-kinetic flux splitting method is designed as an adaptive parameter according to the smoothness of the magnetic pressure to control numerical dissipation. Numerical examples demonstrate that the proposed method can achieve high numerical accuracy, track and resolve strong shock waves in ideal MHD problems. We implement both the projection correction and the central difference correction for the capturing of divergence free magnetic field. Although the former one is time-consuming, it is more robust and oscillation-free than the latter one. Fig. 12 is the results from the central difference correction method, where oscillatory solutions can be obviously observed.

Acknowledgments Huazhong Tang was partially supported by the National Basic Research Program under the Grant 2005CB321703, the National Natural Science Foundation of China (No. 10925101 and No. 10828101), the Doctoral Program of the Education Ministry of China (No. 20070001036), and the Program for New Century Excellent Talents in University (No. NCET-07-0022). K. Xu was supported by Hong Kong Research Grant Council 621709, National Natural Science Foundation of China (Project No. 10928205), and National Key Basic Research Program (2009CB724101).

References

[1] N. Aslan, *Computational investigations of ideal MHD plasmas with discontinuities* , PhD thesis, Nuclear Engineering Department, University of Michigan, 1993.

[2] N. Aslan, *MHD-A: A fluctuation splitting wave model for planar magneto-hydrodynamics*, J. Comput. Phys., vol. 153(1999), pp.437–466.

[3] J. Balbás, E. Tadmor, and C.C. Wu, *Non-oscillatory central schemes for one- and two-dimensional MHD equations. I.*, J. Comput. Phys., vol. 201(2004), pp.261–285.

[4] D.S. Balsara, *Divergence-free adaptive mesh refinement for magnetohydro-dynamics*, J. Comput. Phys., vol. 174(2001), pp.614–648.

[5] D.S. Balsara, *Second order accurate schemes for magnetohydrodynamics with divergence-free reconstruction*, Astrophys. J. Suppl., vol. 151(2004), pp.149–184.

[6] D.S. Balsara and D.S. Spicer, *A staggered mesh algorithm using high order Gudunov fluxes to ensure solenoidal magnetic fields in magnetohydrodynamics simulations*, J. Comput. Phys., vol. 149(1999), pp.270–292.

[7] J.U. Brackbill and D.C. Barnes, *The effect of nonzero div***B** *on the numerical solution of the magnetohydrodynamic equations*, J. Comput. Phys., vol. 35(1980), pp.426–430.

[8] M. Brio and C.C. Wu, *An upwind differencing schemes scheme for the equations of ideal magnetohydrodynamic equations*, J. Comput. Phys., vol. 75(1988), pp.400–422.

[9] D.A. Clarke, *A search for the effects of active magnetic fields in extra-galactic radio sources*, Ph.D. Thesis, New Mexico University, Albuquerque, 1988.

[10] J.P. Croisille, R. Khanfir, and G. Chanteur, *Numerical simulation of the MHD equations by a kinetic-type method,* J. Sci. Comput., vol. 18(1995), pp.481–492.

[11] W.L. Dai and P.R. Woodward, *A simple finite difference scheme for multidimensional magnetohydrodynamical equations*, J. Comput. Phys., vol. 142(1998), pp.331–369.

[12] C.R. Evans and J.F. Hawley, *Simulation of magnetohydrodynamic flows–A constrained transport method*, Astrophys. J., vol. 332(1988), pp.659–677.

[13] J.Q. Han, *An adaptive moving mesh method for two-dimensional ideal magnetohydrodynamics and shallow water magnetohydrodynamics*, Master thesis, School of Mathematical Sciences, Peking University, P.R. China, 2006.

[14] J.Q. Han and H.Z. Tang, *An adaptive moving mesh method for multidimensional ideal magnetohydrodynamics*, J. Comput. Phys., vol. 220(2007), pp. 791–812.

[15] G.S. Jiang and C.C. Wu, *A high–order WENO finite difference scheme for the equation of ideal magnetohydrodynamics*, J. Comput. Phys., vol. 150(1999), pp.561–594.

[16] O.S. Jones, U. Shumlak and D.S. Eberhardt, *An implicit scheme for nonideal magnetohydrodynamics*, J. Comput. Phys., vol. 130(1997), pp.231–242.

[17] S.T. Li, *An HLLC Riemann solver for magneto-hydrodynamics*, J. Comput. Phys., vol. 203(2005), pp.344–357.

[18] R.S. MYONG AND P.L. ROE, *On Godunov–type schemes for magnetohydrodynamics. I. A model system*, J. Comput. Phys., vol. 147(1998), pp.545–567.
[19] K.G. POWELL, *An approximate Riemann solver for magnetohydrodynamics (that works in more than one dimensions)*, ICASE Report No. 94-24, Langley, VA, 1994.
[20] K.G. POWELL, P.L. ROE, T. LINDE, T.I. GOMBOSI, AND D.L. DEZEEUW, *A solution-adaptive upwind scheme for ideal magnetohydrodynamics*, J. Comput. Phys., vol. 154(1999), pp.284–309.
[21] J.A. ROSSMANITH, *A high-resolution constrained transport method with adaptive mesh refinement for ideal MHD*, Comput. Phys. Comm., vol. 164(2004), pp.128–133.
[22] D. RYU, T.W. JONES, AND A. FRANK, *Numerical magnetohydrodynamics in astrophysics: Algorithm and tests for multi-dimensional flow*, Astrophys. J., vol. 452(1995), pp.785–796.
[23] D.D. SCHNACK, I. LOTTATI, Z. MIKIE AND P. SATYANARAYANA, *A finite-volume algorithm for three-dimensional magnetohydrodynamics on an unstructured adaptive grid in axially symmetric geometry*, J. Comput. Phys., vol. 140(1998), pp.71–121.
[24] C.W. SHU AND S. OSHER, *Efficient implementation of essentially non-oscillatory shock capturing schemes*, J. Comput. Phys., vol. 77(1988), pp.439–471.
[25] T. TANAKA, *Finite volume TVD scheme on an unstructured grid system for three–dimensional MHD simulations of inhomogeneous systems including strong background potential field*, J. Comput. Phys., vol. 111(1995), pp.81–92.
[26] H.Z. TANG AND K. XU, *A high-order gas-kinetic method for multidimensional ideal magnetohydrodynamics*, J. Comput. Phys., vol. 165(2000), pp.69–88.
[27] G. TÓTH, *The $\nabla \cdot B = 0$ constraint in shock-capturing magnetohydrodynamics codes*, J. Comput. Phys., vol. 161(2000), pp.605–652.
[28] G. TÓTH AND D. ODSTRCIL, *Comparison of some flux corrected transport and total variation diminishing numerical schemes for hydrodynamic and magnetohydrodynamic problems*, J. Comput. Phys., vol. 128(1996), pp.82–100.
[29] R. TOUMA AND P. ARMINJON, *Central finite volume schemes with constrained transport divergence treatment for three-dimensional ideal MHD*, J. Comput. Phys., vol. 212(2006), pp.617–636.
[30] B. VAN LEER, *Towards the ultimate conservative difference schemes V. A second-order sequel to Godunov's method*, J. Comput. Phys., vol. 32(1979), pp.101–136.
[31] K. XU, *Gas-kinetic theory based flux splitting method for ideal MHD equations*, J. Comput. Phys., vol. 153(1999), pp.334–352.
[32] K. XU, *A gas-kinetic BGK scheme for the Navier-Stokes equations, and its connection with artificial dissipation and Godunov method*, J. Comput. Phys., vol. 171(2001), pp.289–335.
[33] A. ZACHARY, A. MALAGOLI, AND P. COLELLA, *A high–order Godunov method for multidimensional ideal magnetohydrodynamics*, SIAM J. Sci. Comput., vol. 15(1994), pp.263–284.
[34] M.J. ZHANG, S.T. YU, S.C. LIN, S.C. CHANG, AND I. BLANKSON, *Solving the MHD Equations by the Space-Time Conservation Element and Solution Element Method*, J. Comput. Phys., vol. 214(2006), pp.599–617.